Journal of Thermal Analysis and Calorimetry (2022) 147:6593–6603
https://doi.org/10.1007/s10973-021-11018-4

The use of dilatometry aiming to evaluate the metallurgical aspect of coil slump in a hot-rolled medium carbon steel

João Lucas Ribeiro e Fernandes[1] · Altair Lúcio de Souza[1] · Geraldo Lúcio de Faria[1]

Received: 23 October 2020 / Accepted: 22 July 2021 / Published online: 8 August 2021

Abstract
The hot coil slump is a recurrent problem in the manufacturing process of medium and high equivalent carbon steel plates. Even with the success of the hot rolling procedure, the posterior coil slump can occur, representing operational disorder and manufacturing cost increase. Some authors point that the coil slump phenomenon can occur due to metallurgical, mechanical and geometric aspects. Preview studies already investigated several possible mechanical and geometric contributions. However, there are few available experimental data about the metallurgical one, that is, the effect of late austenite decomposition during, or after the coiling stage. In this context, this paper presents a study about the application of dilatometry technique aiming to evaluate the influence of late phase transformations as a relevant cause of a medium carbon steel coil slump. Heating cycles that simulated, with good agreement, some possible plate cooling conditions and isothermal coiling procedures were performed in standardized specimens using a quenching dilatometer. Different combinations of cooling rates and coiling temperatures were evaluated. It was possible to conclude that the dilatometry technique application is viable and efficient to evaluate the metallurgical contribution to the coil slump phenomenon. For the studied steel, it was possible to suggest that a decrease of the cooling rate, in association with a slight decrease of coiling temperature, can significantly suppress the metallurgical influence on the coil slump occurrences.

Keywords Dilatometry · Coil slump · Medium carbon steel · Phase transformations

Introduction

Nowadays, the hot strip manufacturing has a great importance of worldwide steel business. Since around half of all steel products is hot-rolled to strip, mills must have great throughput and availability combined with geometric precision, being able to produces well planned steel microstructures with optimized mechanical properties. In this context, the hot strip mills (HSM) represents an important technology that can produce thin steel plates, up to 0.8 mm thick, with well-designed geometric and microstructural characteristics. There are several HSM layouts, and they vary according to the company's business strategy, available industrial area, available technology, manufacturing capacity and available raw material. Despite the system specificities, in general, the manufacturing flows of hot-rolled strips are similar and consists of roughing steps, followed by finishing rolling, accelerated cooling in a controlled system and, finally, the coiling, with the aim to promote the efficient product storage and shipping to the customer [1–15].

Hot-rolled steel strips are usually stored as coils that are raw materials for several subsequent processes, such as cold rolling, drawing, bending, among others. In order to be further processed, it is necessary that coil central axis fits into equipment that will decoil them (decoiler). For this reason, it is very important that its geometry is as close as possible to a cylinder. When the geometry of the coil cross section is not circular, a defect in the product is considered to occur, which is named coil slump. In general, when the difference between orthogonal diameters in the cross section of the coil is greater than 50 mm, the coil is considered as slumped [9–11, 16, 17].

The technical literature points to three main aspects that contribute to the steel coil slump phenomenon; they are: mechanical, geometric and metallurgical [18–22]. After the strip hot-rolling, it is subjected to the accelerated cooling system where the steel strip is cooled until to the coiling

✉ Geraldo Lúcio de Faria
geraldolfaria@yahoo.com.br

[1] Campus Universitário do Morro do Cruzeiro, Universidade Federal de Ouro Preto, Ouro Preto, MG 35400-000, Brazil

temperature. The purpose of this controlled cooling is to promote the austenite decomposition in order to obtain the desired transformation products, generally a refined microstructure consisting of ferrite and pearlite in the case of medium carbon steels [5, 16, 17, 21]. However, if this transformation does not finish completely during the cooling stage, part of the austenite may decompose during, or after the coiling procedure. According to Cardoso et al. and other researchers, the molar volume of austenite is significantly lower than the ferrite one and, if this transformation occurs during, or after coiling, an abrupt volume increase will occur in the mechanically tensioned coil and this will significantly contribute to the slump phenomenon, constituting thus the metallurgical component of the event [21, 23–25].

When coil slump occurs, even though the transformation of austenitic decomposition has already completely occurred in the accelerated cooling stage, its causes are exclusively due to mechanical and geometric factors. Some authors have already studied these aspects and have shown that they become very significant in very thin strip, and/or very heavy steel coils. It is agreed that these two characteristics facilitate the coil plastic deformation when moved, or when horizontally stored in the industrial storage yards. Even though there are numerous publications on coil winding models, not much literature is available on coil slump. The modelling of coil slump is much more difficult, since the coil can no longer be treated as an axisymmetrical problem. In this scenario, one common method to work with this loss of symmetry is the Finite Element Analysis (FEA) that allows to calculate the coil stresses and its final deformation [21, 22, 26–29]. Park et al. [29] stated that the main mechanical aspect which contributes to the coil slump is the discontinuous stress concentration on the coil. According to them, this may occur due to a coil deflection at the beginning of the coiling procedure. According to Gorni and Silva [21], this discontinuous stress distribution along the coil diameter strongly influences the coil slump due to the fact that the transverse moment of inertia of a coil with very cohesive turns will be greater than that of loose turns.

As a way to decrease the influence of geometric and mechanical factors in the coil slump phenomenon, some authors suggest the increase of the coiling tension. The maintenance of the external turns with temperatures between 150 and 200 °C above the temperatures of the internal turns is also pointed. According to researchers, if this happens, the volumetric contraction of the external turns during the coil cooling would help in the internal turns cohesion, improving the coil integrity [18–22]. Park et al. [29] suggest the use of a sleeve system between the coil and the coiler mandrel to ensure the coil is not initially deflected. Other authors, using basic mechanical theory and FEA, developed optimized mathematical models for control coiling operating conditions aiming to avoid the occurrence of geometric and mechanical problems. Most of these improvements are nowadays implemented in operational programs of industrial hot-rolled strip coilers and are worldwide used [10, 17–22, 29–35].

Despite the several developments and efforts to minimize the mechanical and geometric effects on the coil slump, some authors stated that, as the metallurgical aspect has a decisive contribution in the phenomenon occurrence in steels with medium and high carbon equivalent, if this aspect is not properly studied and controlled, even applying optimized mechanical and geometric adaptations, the coils of medium carbon steels will be strongly susceptible to slump. Volumetric variations in the coil turns, as a result of the late austenite decomposition, are not considered in most mechanical models and, therefore, represent an important stress unbalance, promoting irregular coil deformation, causing its slumping, even if all other mechanical and geometric aspects have been met [17–21].

In this context, the present work proposed to use the experimental dilatometry technique to simulate accelerated cooling cycles and coiling beginning in a medium carbon steel, instantly monitoring the relative length variation of steel specimens. This method was proposed with the aim to allow fine adjustments in the thermal profiles of the steps that precede the strip coiling. This study was performed considering the SAEJ403 1050 chemical composition and the operational limitations of an industrial Steckel mill. In Latin America, industrial and confidential reports describe several occurrences of coil slump for the studied steel when hot-rolled in Steckel mill, even under optimized geometric and mechanical coiling conditions, thus being the late austenite decomposition the possible main cause for coil slumping. For the steel studied in this work, the most reported cases about coil slump led to the coil disposal, representing significant operational and financial losses.

Materials and methods

Materials

The sample studied in this work was taken from a 30 mm thick hot-rolled plate. It is important to highlight that the rolling procedures was performed in a Steckel mill and the steel sample were collected after the finishing rolling procedure, but before the cooling table, i.e. the plate was not submitted to the accelerated cooling system, being cooled in natural air. The chemical composition of the studied steel meets the SAEJ403 [36] requirements for a 1050 grade flat steel (Table 1). It can be seen that it is a common medium carbon steel with C and Mn contents, respectively, of 0.52% and 0.69%; which guarantees an intermediate hardenability.

Table 1 Chemical composition of the studied steel (mass/%)

C	Mn	P	S	Si	Ni	Cr
0.52	0.69	0.014	0.008	0.22	0.01	0.01

Experimental procedures

Initially, the studied steel was characterized in its initial state applying optical microscopy and Vickers microhardness techniques. Representative steel samples were metallographically prepared according to ASTM E3 standard [37], and were chemically etched with Nital 2%. The optical microscopy images were acquired using a LEICA DM2700M optical microscope (OM). The Vickers microhardness tests were performed on a Pantec model HXD 1000TM equipment with 300gf and 15 s of load application time. The previous austenite grain size was estimated applying the automatic equivalent diameter method according to ASTM E112 and ASTM E1382 procedures [38, 39].

Dilatometry specimens were machined in a massive cylindrical geometry (length: 10 mm, diameter: 3 mm) and dilatometry tests were performed on a R.I.T.A. L78 Linseis equipment with the following objectives: (1) Determination of the critical temperatures Ac_1 and Ac_3; (2) Determination of the steel continuous cooling transformation diagram (CCT); (3) Execution of physical simulations of thermal profiles corresponding to the strip accelerated cooling until the coiling beginning, aiming to evaluate the occurrence of late austenitic decomposition.

With the aim to determine the Ac_1 and Ac_3 temperatures, six specimens were heated from room temperature to 900 °C, with a heating rate of 5 °C s^{-1}. The specimens remained at 900 °C for one minute (60 s). By using the derivative method applied to the dilatometric data, the referred critical temperatures were determined [23, 40–42].

For the CCT diagram determination, six specimens were heated under the same above mentioned conditions and then cooled to room temperature with different cooling rates, which were: 1 °C s^{-1}, 5 °C s^{-1}, 15 °C s^{-1}, 23 °C s^{-1}, 50 °C s^{-1} and 150 °C s^{-1}. In the studied case, the medium carbon hot rolling process started by raising the steel temperature above its upper critical Ac_3 temperature, i.e., above the recrystallization temperature. Then controlled load steps were applied, forming the material to the desired profile and specification. While the material was rolled, its temperature was monitored to make sure it remained above the recrystallization temperature. The austenite grains got deformed/elongated in the rolling direction. However, these elongated grains started recrystallizing as soon as they come out from the deformation zone, getting smaller after each deformation step [16, 21, 43].

In this context, it is clear that in a conventional medium carbon hot rolling process, the austenitic grain is refined due to the austenite recrystallization and, for this reason, the average size of the austenitic grains from which the accelerated cooling stage starts is relatively small. As in the dilatometry tests, a strain cell was not used, the austenitizing conditions were defined in order to obtain a small austenitic grain size, justifying the used heating rate, the austenitizing temperature and the applied soaking time. The critical temperatures Ar_1 and Ar_3 were determined, for each studied cooling rate, also applying the derivative method to the experimental data [23, 40, 41].

After dilatometry tests to determine the steel CCT diagram, the tested samples were metallographically prepared and etched with Nital 2% for microstructural characterization. The LEICA model DM 2700 M optical microscope (OM) and the VEGA 3 Tescan scanning electron microscope (SEM) were used for this purpose. After the microstructural characterization, the samples were submitted to Vickers microhardness tests. Ten random measurements were performed in each sample. A test load of 300gf and a test time of 15 s were used. The equipment used in this step was a Pantec, model HXD 1000TM. For the studied austenitizing condition, the prior austenite grain size was measured applying ASTM E112 and ASTM E1382 procedures to the Teepol (240 mL of distillated water, 2 mL of HCl, 2 g of picric acid and 0.5 mL of a surfactant) etched samples, aiming to confirm the success of the proposed method seeking to achieve small austenitic grains [38, 39].

As described in the introductory section, this study proposed to use the dilatometry technique as a tool to evaluate if, for the specific hot-rolling, controlled cooling and coiling scenario currently applied to the SAEJ403 1050 steel, the late austenite decomposition can be a relevant contributing metallurgical aspect to coil slump phenomenon. This research focused on the medium carbon steel submitted to a conventional hot-rolling in a Steckel mill. It is important to highlight that the studied steel strips are often cooled from the last deformation step to the usual coiling temperature (600 °C) with the average cooling rate of 23 °C s^{-1} (Coiling 1 in Table 2). According to the industrial manufacturing planning, these conditions provided the best microstructure-properties-productivity relations. However, applying them, the coil slump occurrence is recurrent, representing significant financial losses. Due to this, there is a great technical and economical need to investigate the occurrence of late austenite decompositions and to evaluate alternative thermal cycles with the aim to avoid the coil slump without to significantly impair the product quality and neither the Steckel mill productivity.

Table 2 Thermal profiles used in the physical simulations of accelerated cooling and coiling beginning

Sample	Cooling rate/°C s^{-1}	Coiling temperature/°C
Coiling 1	23	610
Coiling 2	10	610
Coiling 3	10	590
Coiling 4	15	580

Seeking to simulate the accelerated cooling and coiling beginning, dilatometry specimens were heated from room temperature to 900 °C with a heating rate of 5 °C s^{-1} and were soaked for 60 s. Subsequently, the samples were cooled to a certain temperature at a constant rate, and kept there for one minute, i.e. enough time to austenite complete decomposes (Table 2). Finally, the samples were cooled at 1 °C s^{-1} until room temperature. The isotherm temperature to which the samples were cooled represents the coiling temperature, and the rates at which the samples were cooled represent the average cooling rate applied to the plate in the accelerated cooling stage, between the rolling end and the coiling beginning. It is important to highlight that the evaluated conditions Coiling 2, Coiling 3 and Coiling 4 were proposed considering the specificities of an industrial Steckel mill, coupled to an accelerated cooling system, aiming to maintain the product quality. The chosen of these parameters obeyed limitations related to rolling speed, strip temperature distribution, optimal mechanical and geometric coiling conditions and rolling productivity.

For each physical simulation condition performed in the R.I.T.A. L78 dilatometer, the relative length variation of the specimens was measured as a temperature and time function. The volumetric expansions arising from the austenite decomposition were monitored and evaluated. If these expansions completely occurred before the isothermal stage, it would mean the austenite decomposition occurred before the coiling beginning, and would not be a relevant metallurgical aspect related to the studied steel coil slump. Otherwise, if part of the expansions occurs during the isotherm, it would mean the volumetric variations arising from late austenite decomposition would represent a significant metallurgical component of coil slump phenomenon.

Results and discussion

Initial state characterization

Figure 1 shows the microstructure of the studied steel in its initial state. It is observed that the structure is constituted of ferrite and pearlite, which is in accordance with its chemical composition and processing history. It is also possible to notice the presence of manganese sulfide inclusions. It is observed that the structure is relatively coarse. This is due to the fact that the sample was taken from a plate that did not pass through the cooling system, having been cooled in the natural air. The prior austenite average size was (35 ± 12) µm. The microhardness of the initial condition was (192 ± 8) HV.

Determination of critical temperatures Ac_1 and Ac_3

The derivative method was used to calculate the critical start and end austenitizing temperatures, measured during the continuous heating of six samples at 5 °C s^{-1}. Figure 2a presents the obtained results. It is observed that the average temperatures Ac_1 and Ac_3 are respectively 714 °C and 855 °C. Due to this obtained values, the chosen austenitizing temperature for the CCT diagram and physical simulations was 900 °C, i.e. 45 °C above the Ac_3. This austenitizing temperature coupled to a relatively fast heating (5 °C s^{-1}) and 60 s soaking time guaranteed a relatively small austenite grain size, as desired. Applying the ASTM E112 and ASTM E1382 procedures [38, 39], it was possible to verify that, for this austenitizing condition, the average austenite grain size

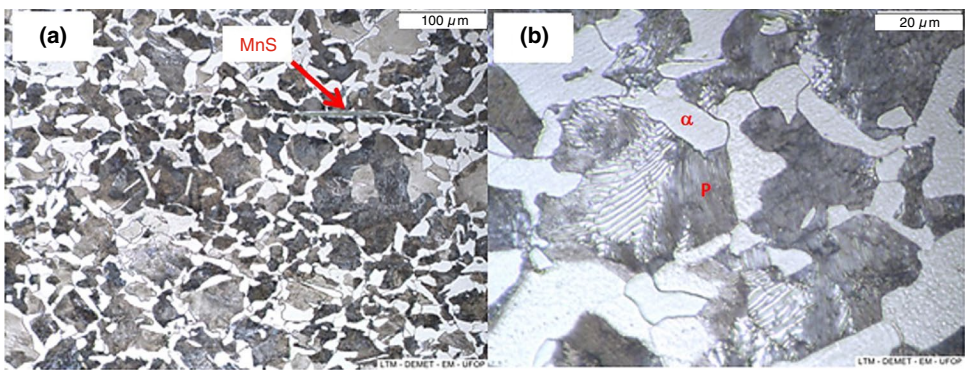

Fig. 1 Microstructure of the studied steel in its initial condition **a** OM-200X, **b** OM-1000x (α-ferrite, P-pearlite)

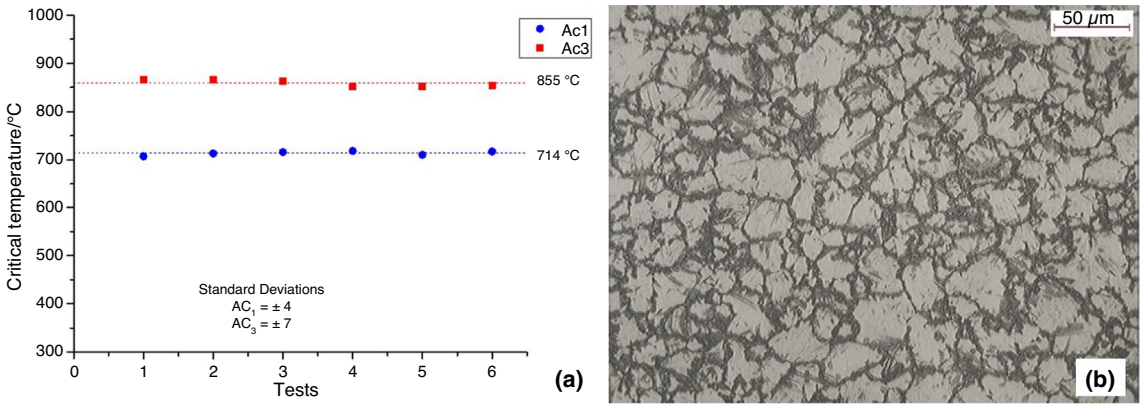

Fig. 2 **a** Austenitizing critical temperatures measured for 5 °C s^{-1} continuous heating; **b** Micrograph illustrating the prior austenite grains revealed by Teepol etching (heating rate: 5 °C s^{-1}, austenitizing temperature: 900 °C, soaking time: 60 s)

was (23 ± 8) µm, i.e. slightly smaller than those verified for as received material, as Fig. 2b illustrates.

Determination of CCT diagram

After determining the critical temperatures Ar_1 and Ar_3 during continuous cooling, for all studied cooling rates, and the Ms temperature for rates where martensitic transformation was observed, it was possible to determine the steel CCT diagram for the studied austenitizing condition. Figure 3 presents the obtained CCT diagram. It was observed that the obtained diagram indicates lower hardenability than the expected for the medium carbon steel SAEJ403 1050 grade, as mentioned in classic heat treatment studies. Considering the carbon content of the studied steel, a diagram shifted to the right was expected. It is assumed that due to the relatively high heating rate, the austenitizing temperature relatively close to Ac_3 and the relatively short soaking time, the previous austenitic grain size was small enough to justify the hardenability loss. Smaller austenitic grains favor the nucleation of diffusional constituents such as ferrite and pearlite, decreasing the steel hardenability [44–48].

Figure 4 presents the microstructures of the samples submitted to the specific cooling rates: 5 °C s^{-1}, 15 °C s^{-1} and 23 °C s^{-1}. Comparing the microstructures of the samples submitted to the dilatometric experiments with that of the initial state, an intense microstructural refining can be observed, confirming one more time the importance of obtaining a small austenitic grain size during the steel austenitizing. It can be seen that for the three cooling rates, the microstructure consists of allotriomorphic ferrite and pearlite. With the cooling rate increase, a decrease in the ferrite fraction was observed, as expected [23, 24, 45–49].

Figure 5 shows the microstructures of the samples submitted to the cooling rates of 50 °C s^{-1} and 150 °C s^{-1}. It

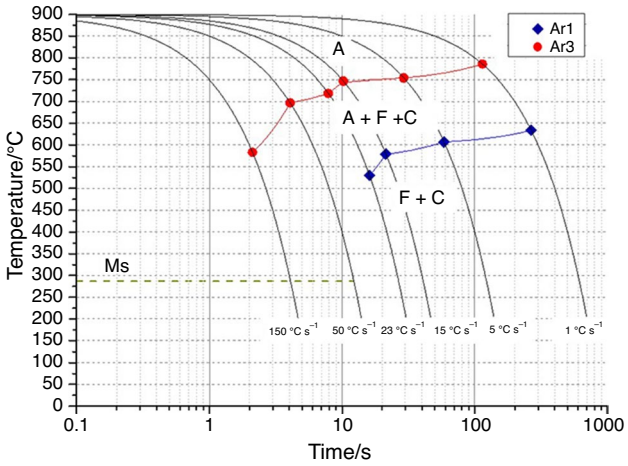

Fig. 3 CCT diagram experimentally determined for the studied steel considering: heating rate—5 °C s^{-1}, austenitizing temperature—900 °C, soaking time—60 s (A-austenite; F-ferrite, C-cementite)

is possible to observe that for 50 °C s^{-1}, the microstructure is mainly constituted by ferrite and pearlite, as consequence of the steel hardenability decrease. However, there is the formation of degenerated pearlite, bainite and small martensite islands aligned to the rolling direction, around manganese sulfide inclusions. In that region, according to technical literature, due to a localized Mn chemical segregation, the atomic diffusion was harmful, favoring the martensite formation [50–52]. It was observed that for 150 °C s^{-1}, the formation of martensite islands occurred more significantly, however the microstructure is mostly constituted by fine pearlite, degenerated pearlite and bainite. Figure 6 presents SEM micrographs highlighting the presence of pearlite, degenerated pearlite, bainite and martensite in sample submitted to 150 °C s^{-1} cooling rate.

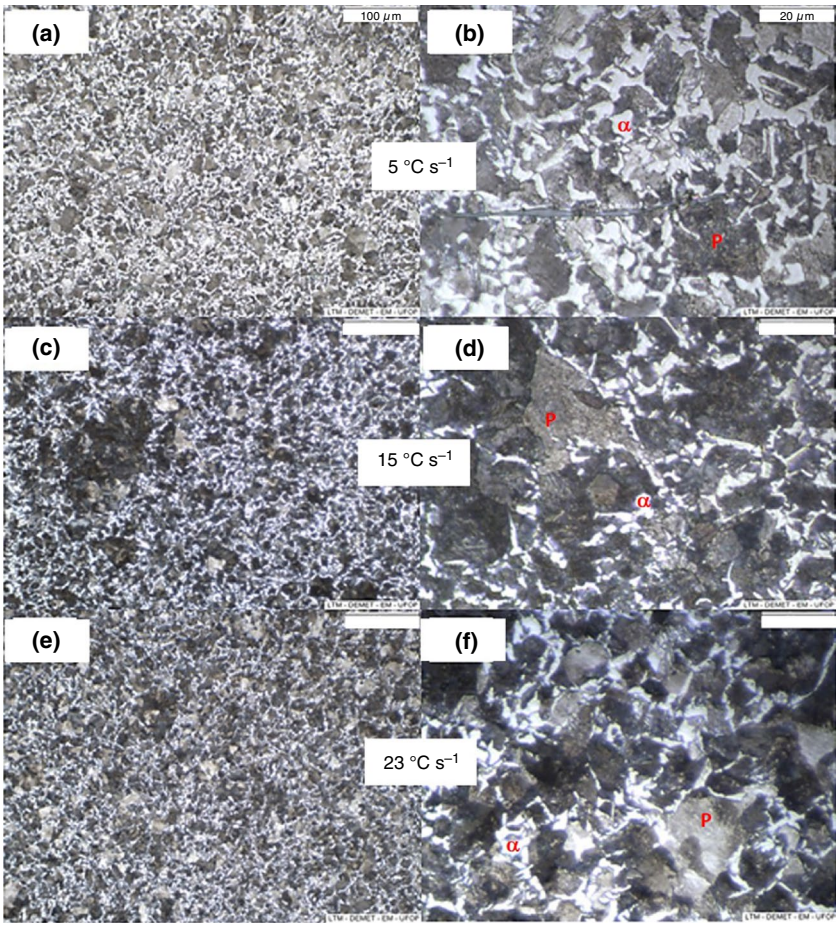

Fig. 4 Microstructures of specimens submitted to 5 °C s^{-1}, 15 °C s^{-1} and 23 °C s^{-1} cooling rates. **a**, **c** and **e** 200x; **b**, **d** and **f** 1000x (α-ferrite, P-pearlite)

Figure 7 presents the Vickers microhardness values of the samples submitted to the studied cooling rates, i.e. 1 °C s^{-1}, 5 °C s^{-1}, 23 °C s^{-1}, 50 °C s^{-1} and 150 °C s^{-1}, as well as the hardness of initial state. As expected, the hardness increased due to the increase in the cooling rate. This observation is in accordance with the characterized microstructures, once increasing the applied cooling rate, the microstructures became more refined, with lower ferrite volumetric fraction and, specifically for 50 °C s^{-1} and 150 °C s^{-1}, martensite islands appeared. It is important to highlight that the presence of martensite islands also justifies the high standard deviation verified for microhadness values measured in samples submitted to 50 °C s^{-1} and 150 °C s^{-1}.

Physical simulation of accelerated cooling until coiling beginning

Using the dilatometric data, it was possible to evaluate the effect of cooling rate on Ar_3 and Ar_1 temperatures. Equation 1, proposed by Cezário et al. [53, 54] was fitted to the experimental data, aiming to establish a mathematical relation between critical temperatures and cooling rate. In Eq. 1, T_c represents the critical temperature and r is the cooling rate. The parameters T_0, α and β are fitting constants. Figure 8 presents the obtained results. It is possible to observe that applying the current cooling rate, i.e. 23 °C s^{-1}, the Ar_3 and Ar_1 temperatures are, respectively, 719 °C and 530 °C. Considering that the actual start coiling temperature is 600 °C, obviously a significant part of austenite decomposition will occur during or after the coiling procedure.

$$T_c = T_0 + \alpha \cdot e^{\beta . r} \quad (1)$$

Figure 9 presents the results about the physical simulation of the accelerated cooling until coiling steps. Figure 9a shows the measured temperature as a time function. About it, some important considerations must be mentioned: (1) the presented temperature values were measured by *k* type thermocouples spot welded in the middle of specimen length; (2) aiming to make easy the data interpretation, the time was parametrized as 0 exactly at the beginning of coiling isotherm, justifying the negative values. Figure 9b highlights the relative length variation of specimens as a time function. These data were instantaneously measured by dilatometry

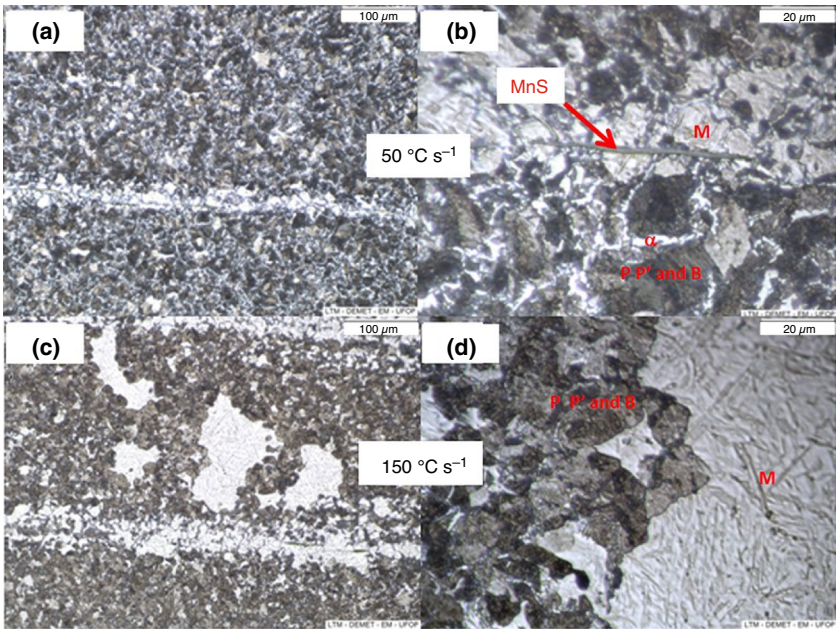

Fig. 5 Microstructures of specimens submitted to 50 °C s^{-1} and 150 °C s^{-1} cooling rates. **a** and **c** 200x; **b** and **d** 1000x (α-ferrite, P-pearlite, P′-degenerated pearlite, B-bainite, M-martensite)

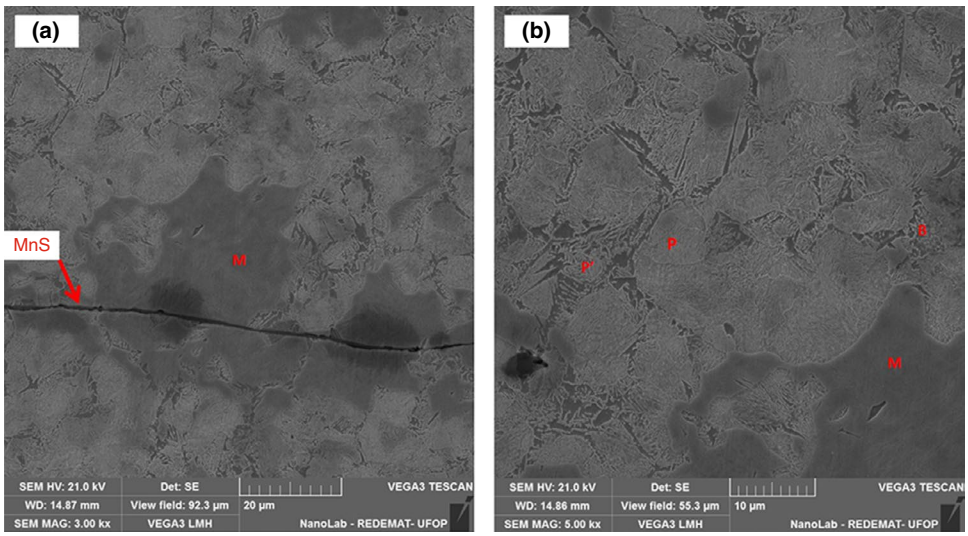

Fig. 6 SEM micrographs of specimens submitted to 150 °C s^{-1} cooling rate. **a** 3000x; **b** 5000x (α-ferrite, P-pearlite, P′-degenerated pearlite, B-bainite, M-martensite)

during the execution of thermal cycles presented in Fig. 9a. In Fig. 9b is possible to verify that, for all studied cooling rates, the specimens contracted linearly to points identified by "*s*", where the volumetric expansions related to the austenite decomposition start. After these expansions (point "f"), with the end of the austenitic decomposition, the specimens again experienced a slight contraction, tending to an asymptotically horizontal behavior over time.

Analyzing Fig. 8, for SAEJ403 1050 steel continuous cooled at 23 °C s^{-1} to room temperature, it was clear that between 719 and 530 °C, an expansion occurs, due to the austenite decomposition. If the cooling stage were interrupted at 610 °C for a coiling procedure, as Fig. 9 presents (Coiling 1), only 53% of all volumetric expansion would take place during the continuous cooling and, therefore, 47% of it would occur during, or after coiling. According to many authors, slightly plate deflections at coiling beginning, promoting discontinuous stress concentration on the coil, contribute too much to the coil slump [21, 22, 26–29]. In this context, it can be stated that considering this current coiling condition applied to SAEJ403 1050 steel, the late austenite decomposition can strongly increase the occurrence of coil slump phenomenon. This relatively simple dilatometric characterization shows that, for this current cooling and coiling thermal profile used in some HSM facilities, even considering optimized mechanical and geometric coiling conditions, the coil slump can occur due to metallurgical motivation, that is late austenite decomposition.

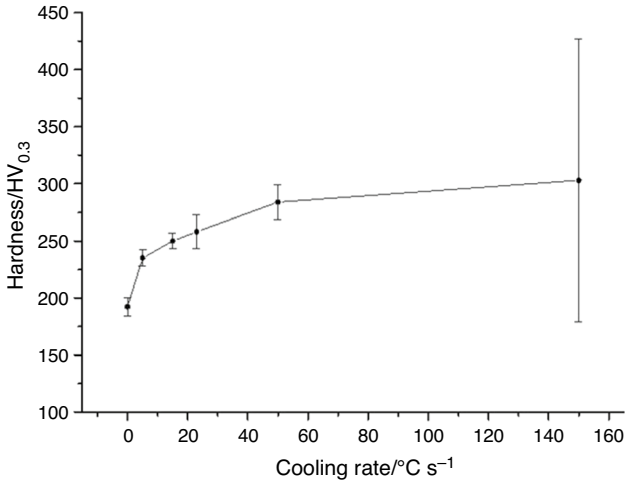

Fig. 7 Effect of cooling rate on the steel Vickers microhardness. The 0 °C s^{-1} rate represents the initial steel condition

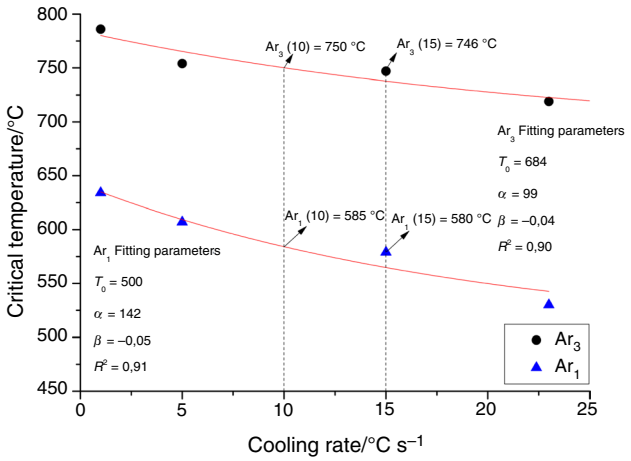

Fig. 8 Effect of cooling rate on steel critical temperatures highlighting the Eq. 1 fitting

In this specific case, with the occurrence of late austenite decomposition, a way to avoid the coil slump phenomenon is to keep the coil tensioned in the mandrel for a longer period of time after coiling, in this way, the microstructural changes could not affect its final shape. However, this action strongly affects the mill productivity and decreases the coiling mandrel life, since the high temperature impairs the equipment lubrication, thus forcing its premature replacement [18].

As Fig. 8 highlights the critical temperatures related to the start and the end of austenite decomposition are sensitive to the cooling rate. The lower the cooling rate, the higher these critical temperatures. Therefore, it was evaluated the effect of the cooling rate decrease on the possibility to anticipate the referred transformation, trying to complete it before the coiling beginning, or at least, to guarantee that only a small fraction of austenite finishes its decomposition late, not significantly affecting the coil volumetric changes [23, 45].

With the aim to maintain the beginning of coiling temperature as 610 °C, regarding Figs. 8 and 9, it was suggested that, after the last rolling step, if SAEJ403 1050 steel plate were submitted to 10 °C s^{-1} cooling rate until the coiling beginning (Coiling 2), the Ar_1 temperature would be around 585 °C and only around 5% of all volumetric expansion would occur during or after the coiling stage. This condition, compared to the Coiling 1, would represent a significant decrease on the metallurgical contribution to the coil slump. However, if the coiling temperature was decreased to 590 °C, maintaining the 10 °C s^{-1} cooling rate (Coiling 3), the austenite decomposition would finish around two seconds before the coiling start. This conditions could eliminate the metallurgical aspect of coil slump for the studied steel. A negative feature of this scenario applying 10 °C s^{-1} after the last rolling step, mainly in Steckel mills, is the need to decrease the rolling speed at the last rolling stage. This routine could significantly impair the mill productivity [1, 5].

Aiming to decrease the possible negative impact on the mill productivity, the Coiling 4 condition was simulated. The cooling rate has been increased to an intermediate value (15 °C s^{-1}), but observing Fig. 8, the proposed coiling temperature was decreased to 580 °C. Considering these parameters, Fig. 9 shows that the full austenite decomposition happens before de coiling. Among the evaluated conditions, this would be the best one, considering the process limitations. According to Rizzo [16] and Kloeckner et al. [55], for medium carbon steels, the coiling temperature cannot be too much lowered. According to them, if coiling temperature decreases, flatness problems can occur. The lower the coiling temperature, the higher the thermal gradient between the center and the edges of the plates, promoting localized plastic deformations due to heterogeneous thermal contractions. This flatness problem is named wavy edge [16, 55, 56].

Considering the SAEJ403 1050 coiling temperature cannot be lower than 580 °C in several mill facilities, with the aim to avoid flatness problems, it is suggested that for this minimum coiling temperature, the safe cooling rate that will not promote significant metallurgical effect contributing to the coil slump is 15 °C s^{-1}. However, it is important to highlight that decreasing cooling rate from 23 to 15 °C s^{-1}, the steel microstructure and mechanical properties will slightly change. Figure 10 presents a comparison between specimens submitted to Coiling 1 and Coiling 4 conditions. It is possible to observe that the microstructure obtained at 15 °C s^{-1} is slightly coarser than the one obtained at 23 °C s^{-1}. The ferrite fractions in samples cooled at 15 °C s^{-1} and 23 °C s^{-1} are, respectively, $(18 \pm 4)\%$ and $(12 \pm 3)\%$. The measured hardness values at 15 °C s^{-1} and 23 °C s^{-1} are respectively (250 ± 6)HV and (257 ± 10)HV. Therefore, in the rolling

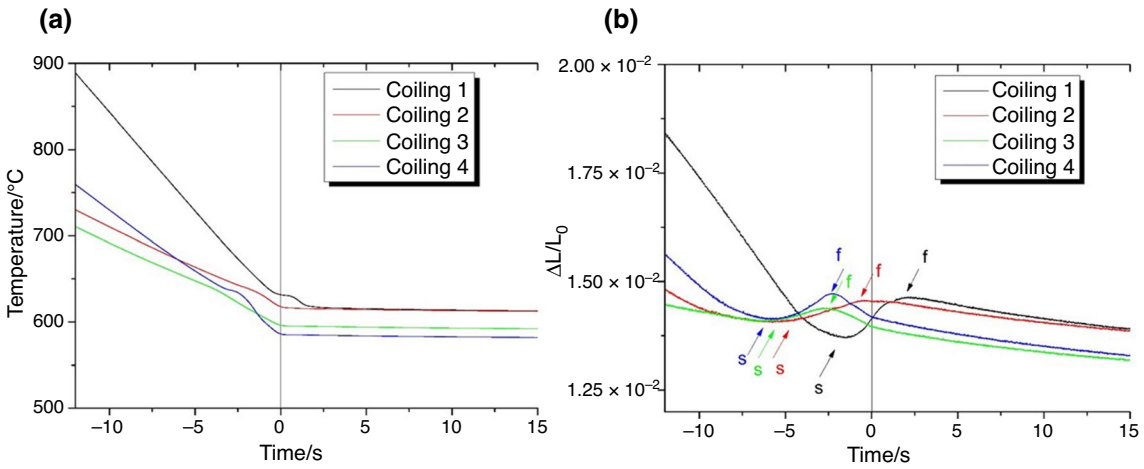

Fig. 9 **a** Thermal profiles measured during the physical simulation; **b** relative length variation as a time function. The 0 s represents the beginning of coiling isotherm; "s" and "f" indicates, respectively, the start and the end of austenite decomposition

planning, it is important to consider that the decrease of the cooling rate from 23 to 15 °C s^{-1} will increase the ferrite fraction in 6% as well as will decrease Vickers Hardness in 3%.

Conclusions

For the SAEJ403 1050 steel continuously heated at 5 °C s^{-1}, the critical austenitizing temperatures Ac_1 and Ac_3 were, respectively, 714 °C and 855 °C. The average austenite grain size measured for a full austenitizing at 900 °C during 60 s was (23 ± 8) µm. The studied steel CCT diagram was experimentally obtained and a mathematical relation between austenite decomposition critical temperatures and cooling rate was established. The generated knowledge made possible to design three alternative thermal profiles of accelerated cooling and coiling beginning with the aim to decrease the effect of late austenite decomposition on coil slump.

The use of the dilatometry technique to evaluate the metallurgical component of the coil slump phenomenon in hot-rolled SAEJ403 1050 steel was efficient. For the studied steel, the physical simulations of the accelerated cooling and coiling beginning showed that: (1) for the cooling rate currently used in hot strip rolling, austenite does not decompose completely before the coiling beginning, i.e. around 47% of volumetric expansion occurs during, or after the coiling; (2) the condition that better suppressed the metallurgical component of the coil slump phenomenon was to decrease the cooling rate to 15 °C s^{-1} and the coiling temperature to 580 °C.

It is important to emphasize that changes in the cooling and coiling parameters cause changes on the steel final microstructure and hardness. For the SAEJ403 1050 steel, it was observed that the decrease from 23 to 15 °C s^{-1} promoted the ferrite fraction increase in 6%, as well as the Vickers hardness decrease in 3%. These changes must be considered in the final product quality control.

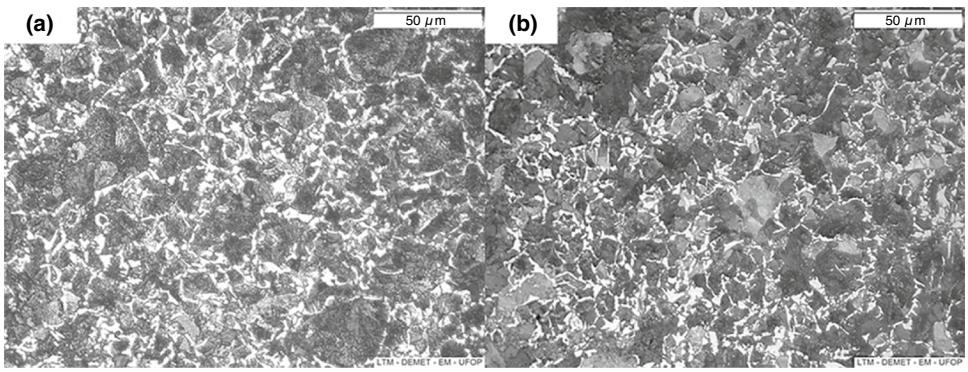

Fig. 10 Microstructures of samples submitted to **a** Coiling 4 (15 °C s^{-1}) and **b** Coiling 1 (23 °C s^{-1}) conditions—500x

Acknowledgements The authors would like to thank the Conselho Nacional de Desenvolvimento Científico e Tecnológico (CNPq) and Universidade Federal de Ouro Preto for the financial support.

Authors' contribution JLReF: Validation, Formal analysis, Investigation. ALdS: Investigation, resources. GLdF: Conceptualization, Methodology, Data Curation, Writing (Original draft, review and editing), Supervision.

Declarations

Conflict of interest The authors whose names are listed in this paper certify that they have no conflicts of interest.

References

1. Kramer S, Kneppe G, Rosenthal D. Technology and performance of modern steckel mills. Iron Steel Eng. 1997;7:17–26.
2. Militzer M, Hawbolt EB, Meadowcroft TR. Microstructural model for hot strip rolling of high-strength low-alloy steels. Metall Mater Trans A. 2000;31A:1247–59.
3. Ouchi C. Development of Steel Plates by intense use of TMCP and direct quenching process. ISIJ Int. 2001;41:542–53.
4. Tamehiro H, Yamada N, Matsuda H. Effect of the thermo-mechanical control process on the properties of high-strength low alloy steel. Trans Iron Steel Inst Jpn. 1985;25:54–61.
5. Lino JJP, Borges JM, Souza AL, Frenn JH, Pereira MM, Schuwarten W, Faria GL. The benefits of using the tapering strategy for rolling load reduction at the heat and tail ends at Steckel mills. Tecnol Metal Mater Min. 2016;13(3):179287.
6. Konovalov YV, Khokhlov AS. Benefits of Steckel mills in rolling. Steel Trans. 2013;43:206–11.
7. Adamczyk J. Development of the microalloyed constructional steels. J Achiev Mater Manuf Eng. 2006;14:9–20.
8. Kurp O, Kukhar VV, Klimov E, Prysiazhnyi AH. Thermomechanical controlled rolling of hot coils of steel grade S355MC at the wide-strip rolling mill 1700. Solid State Phenom. 2019;291(1):63–71.
9. Maubane R, Banks KM, Tuling AS. Hot strength during coiling of low c and nb-microalloyed steels. In: HSLA Steels 2015, Microalloying 2015 and Offshore Engineering Steels; 2015.
10. Razinkov J, Minichmayer R, Schmoller FX, Seilinger A. Innovations for coiling of modern hot rolled flat materials. Metall Min Ind. 2011;3(7):32–8.
11. El-Shenawy E, Reda R. Optimization of TMCP strategy for microstructure refinement and flow-productivity characteristics enhancement of low carbon steel. J Mater Res Technol. 2019;8(3):2819–31.
12. Gong P, Palmiere EJ, Rainforth WM. Thermomechanical processing route to achieve ultrafine grains in low carbono microalloyed steels. Acta Mater. 2016;119:43–54.
13. Mandal S, Tewary NK, Ghosh SK, Chakrabarti D, Chatterjee S. Thermo-mechanically controlled processed ultrahigh strength steel: microstructure, texture and mechanical properties. Mater Sci Eng A. 2016;663:126–40.
14. Jiang J, Bao W, Peng ZY, Wang YB, Liu J, Dai XH. Experimental investigation on mechanical behaviors of TMCP high strength steel. Constr Build Mater. 2019;200:664–80.
15 Uranga P, Rodriguez-Ibabe JM. Thermomechanical processing of steels. Metals. 2020. https://doi.org/10.3390/met10050641.
16. Rizzo EMS. Processos de laminação a quente de produtos planos de aço. São Paulo: Associação Brasileira de Metalurgia, Materiais e Mineração. 2011.
17. Lima Jr SOL, Martins JBR, Prado AC, Volpato LFS, Silva CN. Redução da ovalização em bobinas a quente de um aço com carbono equivalente maior do que 0,58 produzido no laminador de tiras a quente da companhia siderúrgica de tubarão. Associação Brasileira de Metalurgia, Materiais e Mineração. In: Anais do 42° Seminário de Laminação, Processos e Produtos Laminados e Revestidos; 2005. Santos, Brazil. São Paulo.
18. Areas VLF, Barbosa GM, Dassie C, Godinho GA, Jacolot R, Marmulev A, Ney VB, Rodrigues FJ. Redução de ovalização em bobinas de aços "dual phase" no LTQ da Arcelormittal Tubarão. In: 51° Seminário de Laminação – Processos e Produtos Laminados e Revestidos. 2014.
19. Cho H, Cho Y, Im Y, Lee JK, Kwak JH, Han HN. A finite element analysis for asymmetric contraction aftercoiling of hot-rolled steel. J Mater Process Technol. 2010;210:907–13.
20. Milenin A, Kustra P, Kuziak R, Pietrzyk M. Model of residual stresses in hot-rolled sheets with taking into account relaxation process and phase transformation. Procedia Eng. 2014;81:108–13.
21. Gorni AA, Silva MRS. Ovalização de bobinas a quente de aços com médio teor de carbono. In: 51° Seminário de Laminação – Processos e Produtos Laminados e Revestidos, 2014.
22. Mazur VL, Meleshko VI, Kostyakov VV, Karetnyi ZP. Shape stability of coils of hot rolled strip. Steel USSR. 1987;17:421–4.
23. Cardoso RA, Faria GL. Characterization of austenite decomposition in steels with different chemical concepts and high potential to manufacture seamed pipes for oil and gas industry. Mater Res. 2019;22(5):e20190378.
24. Kaspar R, Kapellner W, Pawelski O. Effect of austenite deformation on the continuous cooling transformation of medium carbon steels. Int J Mater Res. 1987;78:569–75.
25. Krishnan K, Singh SB, Sahay SS. Modeling non-isothermal austenite to ferrite transformation in low carbon steels. Mater Sci Eng A. 2007;445–446:310–5.
26. Li S, Cao J. A hybrid approach for quantifying the winding process and material effects on sheet coil deformation. Am Soc Met. 2004;126:304–13.
27. Smolinski P, Miller CS, Marangoni RD, Onipede D. Modeling the collapse of coiled material. Finite Elem Anal Des. 2002;38:521–35.
28. Belskii SM, Shopin II. Stress-strain state of coiled steel. Steel Trans. 2017;47(1):722–7.
29. Park Y, Park K, Won S, Hong W, Park H. Stress analysis model of strip winding with a sleeve for a coil of thin stainless steel. J Iron Steel Res Int. 2017;24:1–7.
30. Jeong CS. The analysis of stress distribution and strain of the strip build-up and the temperature gradient in coiling process. Pusan: Pusan National University; 2001.
31. Choi YJ. PID Sliding mode control using a coiler simulator in hot strip mill. Pusan: Pusan National University; 2008.
32. Choi Y, Lee M. A downcoiler simulator for high performance coiling in hot strip mill lines. Int J Precis Eng Manuf. 2009;10:53–61.
33. Pholdee N, Sujin B, Park W, Kim D, Im Y, Kwon H, Chun M. Optimization of flatness of strip during coiling process based on evolutionary algorithms. Int J Precis Eng and Manuf. 2015;16:1493–9.
34. Pholdee N, Park W, Kim D, Im Y, Bureerat S, Kwon H, Chun M. Efficient hybrid evolutionary algorithm for optimization of a strip coiling process. Eng Optim. 2015;47(4):521–32.
35. Wang Y, Li L, Yan X, Luo Y, Wu L. Modeling of stress distribution during strip coiling process. J Iron Steel Res Int. 2012;19:6–11.
36. SAE.J403: Chemical compositions of SAE carbon steels. Pittsburgh: SAE International; 2014.

37. ASTM E3-11. Standard guide for preparation of metallographic specimens. ASTM International; 2017.
38. ASTM E112-1. Standard test methods for determining average grain size. ASTM International; 2013.
39. ASTM E1382-97. Standard test methods for determining average grain size using semiautomatic and automatic image analysis. ASTM International; 2015.
40. Pawlowski B. Determination of critical points of hypoeutectoid steels. Archiev Metall Mater. 2012;57:957–62.
41. Faria GL, Paula JMA, Lima MSF. Characterization of phase transformations and microstructural changes in an API 5CT L80 steel grade during Ni alloy cladding. Mater Res. 2018;21(5):e20180294.
42. Moravec J, Nováková I, Vondrácek J. Influence of heating rate on the transformation temperature change in selected steel types. Manuf Technol. 2020;20(2):217–22.
43. Balogun SA, Lawal GI, Sekunowo OI, Adeosun SO. Influence of finishing temperature on the mechanical properties of conventional hot rolled steel bar. J Eng Technol Res. 2011;3(11):307–13.
44. Bhadeshia HKDH, Yang HS. Austenite grain size and the martensite-start temperature. Scr Mater. 2009;60:493–5.
45. Esmailian M. The Effect of cooling rate and austenite grain size on the austenite to ferrite transformation temperature and different ferrite morphologies in microalloyed steels. Iran J Mater Sci Eng. 2010;7:7–14.
46. Çakir M, Özsoy A. Investigation of the correlation betwee thermal properties and hardenability of Jominy bars quenched with air-water misxture for AISI 1050 steel. Mater Des. 2011;32:3099–105.
47. Zhao H, Palmiere EJ. Effect of austenite grain size on acicular ferrite transformation in a HSLA steel. Mater Charact. 2018;145:479–89.
48. Wu BB, Wang XL, Wang ZQ, Zhao JX, Jin YH, Wang CS, Shang CJ, Misra RDK. New insights from crystallography into the effect of refining prior austenite grain size on transformation phenomenon and consequent mechanical properties of ultra-high strength low alloy steel. Mater Sci Eng A. 2019;745:126–36.
49. Olasolo M, Uranga P, Rodriguez-Ibabe JM. Effect of austenite microstructure and cooling rate on transformation characteristics in a low carbon nb-v microalloyed steel. Mater Sci Eng A. 2011;528:2559–69.
50. Grajcar A, Kaminska M, Opiela M, Skrzypczyk P, Grzegorczyk B, Kalinowska-Ozgowicz E. Segregation of alloyinh elements in the thermomechanically rolled medium-Mn multiphase steels. J Achiev Mater Manuf Eng. 2012;55(2):256–64.
51. Pichler A, Traint S, Hebesberger T, Stiaszny P, Werner EA. Processing of thin multiphase steel grades. Steel Res Int. 2007;78:216–23.
52. Domitner J, Kharicha A, Grasser M, Ludwig A. Reconstruction of three-dimentional dendritic structures based on the investigation of microsegregation patterns. Steel Res Int. 2010;81(8):644–51.
53. Cezário ALS, Porcaro RR, Faria GL. Proposition of an empirical model for determination of critical temperatures during continuous cooling in heat affected zones of IF steels welded by the TIG process. Rev Soldagem Inspeção. 2019;24:e2420.
54. Cezário ALS, Faria GLF. Proposition of an empirical functional equation to predict the kinetics of austenite to ferrite transformation in a continuous cooled IF-Ti-stabilized steel. Mater Res. 2021;24(2):e20200498.
55. Kloeckner HJ, Silva CN. Demag technical assistance for flatness—final report. CST-Arcelor Brasil; 2006.
56. Cho H, Cho Y, Kim D, Kim S, Lee W, Han HN. Finite element investigation for edge wave prediction in hot rolled steel during run out table cooling. ISIJ Int. 2014;54:1646–52.